

UV-TO-IR SPECTRAL ENERGY DISTRIBUTIONS OF GALAXIES AT $Z > 1$: THE IMPACT OF *HERSCHEL* DATA ON DUST ATTENUATION AND STAR FORMATION DETERMINATIONS

V. Buat¹, S. Heinis² and M. Boquien¹

Abstract. We report on our recent works on the UV-to-IR SED fitting of a sample of distant ($z > 1$) galaxies observed by *Herschel* in the CDFS as part of the GOODS-*Herschel* project.

Combining stellar and dust emission in galaxies is found powerful to constrain their dust attenuation as well as their star formation activity.

We focus on the characterisation of dust attenuation and on the uncertainties on the derivation of the star formation rates and stellar masses, as a function of the range of wavelengths sampled by the data and of the assumptions made on the star formation histories

Keywords: High-redshift galaxies, galaxy evolution, photometry

1 Introduction

Star formation rates (SFR) and stellar masses (M_{star}) are the main parameters estimated from large samples of galaxies and they are commonly used to constrain their star formation history and the evolution of their baryonic content. The slope and dispersion of the relation found between SFR and M_{star} both at low and high redshift (e.g. Brinchmann et al. 2004; Noeske et al. 2007; Rodighiero et al. 2011) directly depends on the measurement accuracy of these parameters.

Two major methods are commonly used to measure SFRs. The first approach consists of using empirical recipes. The SFR is deduced by applying conversion factors between an observed emission coming mostly from young stars and the SFR (e.g. Kennicutt 1998). Another widespread method is to exploit the full panchromatic information available for a given sample by fitting the spectral energy distributions (SEDs). The coupling stellar (UV-optical) and dust (mid and far-IR) has proven to be particularly powerful to measure SFRs and overcome the issue of dust attenuation, either with empirical recipes (e.g. Kennicutt & Evans 2012, for a review) or with physically motivated fitting codes (da Cunha et al. 2008; Noll et al. 2009). However the impact of the star formation history remains an open issue, especially at high redshift or in extreme objects (Kobayashi et al. 2013; Schaerer et al. 2013).

M_{star} derivations are almost insensitive to dust attenuation but strongly depend on the assumed stellar population synthesis model and star formation history (e.g. Papovich et al. 2001; Pforr et al. 2012; Maraston et al. 2010). For a given set of assumptions about the stellar population synthesis model, including metallicity and star formation history, and adopting an initial mass function, the stellar masses are robustly estimated. However systematic differences appear when different assumptions are made and these input parameters are either non or very poorly constrained (e.g. Marchesini et al. 2009). The uncertainty about the star formation history itself induces large variations in stellar mass derivation (Bell et al. 2003; Pforr et al. 2012).

2 Datasets and tools

2.1 Observations and sample used

We select galaxies in the GOODS-S field with accurate measurements of the UV, visible, NIR and IR rest frame emissions. We start with the multi-wavelength catalogue of Cardamone et al. (2010), which includes the GOODS

¹ Aix-Marseille Universit , CNRS, LAM (Laboratoire d'Astrophysique de Marseille) UMR7326, 13388, Marseille, France

² Department of Astronomy CSS Bldg., Rm. 1204, Stadium Dr. University of Maryland College Park, MD 20742-2421

Spitzer IRAC and MIPS data. In addition to broad band optical data, deep intermediate-band imaging from the Subaru telescope provide photometry with fine wavelength sampling and estimate more accurate photometric redshifts. We restrict the field to the $10' \times 10'$ observed by the PACS instrument (Poglitsch et al. 2010) on board of the *Herschel* Space Observatory (Pilbratt et al. 2010) at 100 and 160 μm , as part of the GOODS-*Herschel* key programme (Elbaz et al. 2011). We refer to Buat et al. (2012) and Buat et al. (2013, A&A submitted) for a detailed description of the collected data. The final sample contains 236 sources with $1 < z < 3$. 32 objects are detected with PACS at 100 and 160 μm , 40 only at 100 μm and 8 only at 160 μm . 28 photometric bands are compiled from U to 24 μm (all the galaxies are detected at 24 μm). The rest-frame luminosity at 1530 \AA of each galaxy is obtained by modelling a power-law between 1300 and 2500 \AA in the rest frame of the sources.

2.2 SED fitting tool: CIGALE

SED fitting is performed with the CIGALE code (Code Investigating GALaxy Emission)* developed by Noll et al. (2009). CIGALE combines a UV-optical stellar SED with a dust component emitting in the IR and fully conserves the energy balance between the dust absorbed stellar emission and its re-emission in the IR. The output parameters are all estimated from their probability distribution function (PDF) with the expectation value and its standard deviation. The input parameters are similar to those used in Buat et al. (2012) except for the star formation histories. For the purpose of the present analysis, we explore several models: single stellar populations exponentially decreasing or increasing and two stellar populations with a recent one on top of an older population created with an exponentially decreasing SFR. All models are built with an age of the creation of the first stars taken either free or fixed ($z_f \simeq 8$). A first, global, comparison of the models is performed by comparing the reduced best-fit χ^2 distribution given by the code as shown in Fig.1. The best-fit χ^2 distributions appear similar for all models but the fixed-age decl.- τ model which is unable to reproduce the data. We also exclude free-age rising- τ models from the following discussions since these models are introduced to increase the age of the stellar populations (Maraston et al. 2010).

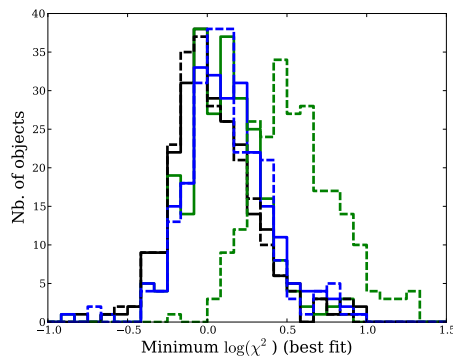


Fig. 1. Distributions of reduced χ^2 values obtained for the best fits and plotted in a logarithmic scale. Black: 2-populations model, green: decl.- τ model, blue: rising- τ model. The solid lines are obtained for models with the age of the stellar population taken free, the dashed lines correspond to a fixed age for the stellar population.

3 SFR and M_{star} determinations

3.1 Full UV-to-IR SEDs

Adopting different star formation histories do not modify SFR measurements (Fig.2, left) with systematic shifts lower than 0.05 dex whereas it has a clear impact on M_{star} determinations (Fig.2, right) with systematic differences reaching 0.3 dex between the most extreme cases. Because of the outshining by young stars, older stellar populations are hidden and τ -models are likely to give only lower limits to the total stellar mass. Models considering an old and young population give higher masses. The very good agreement found between SFR determinations with either a single stellar population or with an over-imposed burst of constant star formation

*<http://cigale.oamp.fr>

should be found surprising. Actually Reddy et al. (2012) have shown that for ages larger than ~ 100 Myr rising- τ models lead to a constant production of the UV light, in the present study stellar populations are older than 2 Gyr for the rising- τ model so we expect a robust determination of the SFR. The effective star formation history we obtain for the decl.- τ model is close to a constant SFR: the t_f/τ ratio is found most of the time lower than 1 and the age of the stellar population is found larger than 100 Myr for 94% of our galaxies, also ensuring a stationarity in the production of the UV light. Therefore the agreement between our SFR estimations is expected. It is worth noticing that the presence of IR data give us a robust measurement of the dust attenuation, allowing us to fit the true intrinsic UV continuum of our galaxies

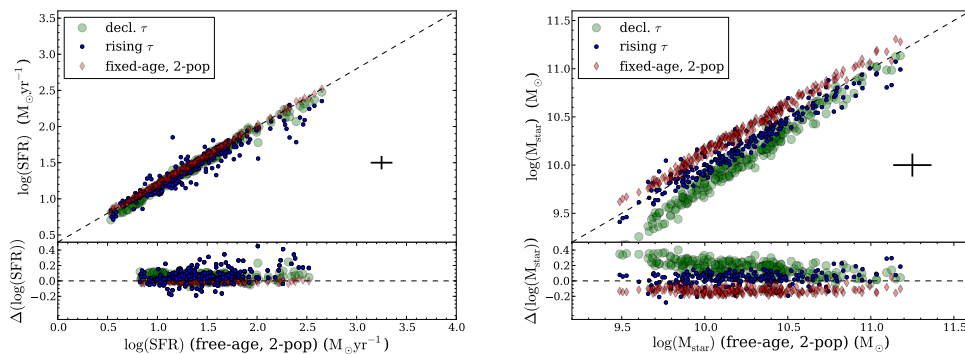


Fig. 2. Comparison of SFR (**left panel**) and M_{star} (**right panel**) determinations from different models. The x-axis is from the baseline model (free-age 2-populations), the y-axis corresponds to free-age decl.- τ (green circles), fixed-age rising- τ (blue dots) and 2-populations (red diamonds) models. Typical uncertainties on parameter estimations are indicated by a black cross. $\Delta(\text{SFR}) = \Delta(\log(\text{SFR}_{2\text{pop}}) - \log(\text{SFR}_{\tau\text{-model}}))$ and $\Delta(M_{\text{star}}) = \Delta(\log(M_{\text{star}\text{-}2\text{pop}}) - \log(M_{\text{star}\text{-}rising\text{-}\tau}))$

3.2 The impact of IR data on SFR determinations

We now perform the SED fitting excluding IRAC4, MIPS and PACS data and considering only the free-age 2 populations model. Without IR data, results substantially change for the parameters linked to the recent star formation. A large dispersion is found between values of SFR estimated with and without IR data (corresponding to 0.65 mag). Omitting IR data strongly affects the accuracy of dust attenuation and SFR with an average uncertainty multiplied by a factor ~ 2 and the distribution of these parameters is found flatter. It is illustrated in Fig. 3 with a strong dependence of the SFR estimates when IR data are not present on the SFR of the galaxies estimated with the whole dataset: assuming that SFRs estimated with the whole dataset are reliable, low SFRs are overestimated and large SFRs underestimated when IR data are missing. Excluding NIR or intermediate band data do not affect significantly the SFR measurements.

Star forming galaxies are often classified as Main Sequence and Starburst galaxies according to the value of their specific SFR ($\text{SSFR} = \text{SFR} / M_{\text{star}}$). The evolution of SSFR with redshift also place constraints on galaxy formation scenarios (e.g. Fontanot et al. 2009). In Fig.3 we show the influence of introducing or not IR data to estimate SSFRs. 30% of the sample exhibit a difference in SSFR which exceeds a factor 2. Such a factor 2 (0.3 dex) is in the order of the dispersion of the Main Sequence measured with IR data (e.g. Noeske et al. 2007; Rodighiero et al. 2011). Starburst galaxies are defined to have a SSFR exceeding by a factor 2 that of a Main Sequence galaxy with the same mass by Elbaz et al. (2011) (note however that Rodighiero et al. (2011) and Sargent et al. (2012) adopt a more conservative ratio of 4 between the SSFR of starburst and Main Sequence galaxies). Indeed, a large uncertainty is expected in the determination of SSFR without IR data for very dusty systems. However in galaxies with a moderate to low dust attenuation ($A_{\text{FUV}} < \sim 3$ mag) SSFR is found overestimated by a factor larger than 2 in 30% of the cases due to an overestimation of A_{FUV} . The percentage reaches 40% for galaxies with $A_{\text{FUV}} < \sim 2$ mag with larger SSFRs found without IR data in 80% of the cases. The variation of the SSFR with z is a matter of debate, especially at high redshift with the presence or not of a plateau in SSFR at $z > \sim 4$ (e.g. Bouwens et al. 2012; Heinis et al. 2013), the analysis being complicated by the presence of intense emission lines in the photometric bands (de Barros et al. 2012). If a substantial dust attenuation occurs at high redshift (Finkelstein et al. 2012) it may well also affect the analysis and ALMA

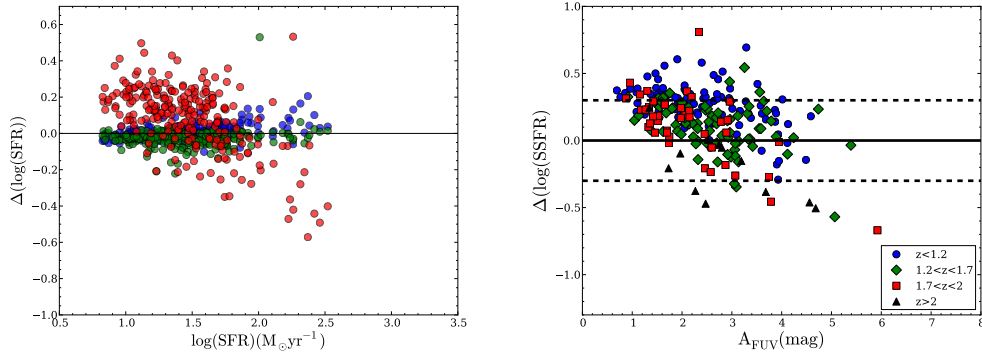


Fig. 3. Left: Comparison between SFR estimations for the free-age 2-populations model with and without optical intermediate bands, NIR and IR data. Xaxis: all the dataset is used. Yaxis: parameters estimated without intermediate band data (blue circles), without NIR data (green circles) and without IR data (red circles). **Right:** Difference between SSFR measured with and without IR data as a function of dust attenuation in FUV for different redshift bins. The solid line correspond to a perfect agreement in both measurements and dotted lines to a factor 2 of difference. $\Delta \log(\text{SFRS}) = \log(\text{SSFR}_{\text{noIR}}) - \log(\text{SSFR}_{\text{alldata}})$.

observations will be mandatory to reliably measure SFRs in these objects as emphasized by Schaerer et al. (2013).

References

- Bell E. F., McIntosh D. H., Katz N., Weinberg M. D., 2003, *ApJS*, 149, 289
 Borch A., Meisenheimer, K., Bell, E., et al., 2006, *A&A*, 453, 869
 Bouwens, R. J., Illingworth, G. D., Oesch, P. A., et al. 2012, *ApJ*, 754, 83
 Brinchmann J., Charlot S., White S. D. M., et al. 2004, *MNRAS*, 351, 1151
 Buat, V., Noll, S., Heinis, S., et al. 2012, *A&A*, 545, 141
 Cardamone, C.N., van Dokkum, P.G., Urry, C.M., et al. 2010, *ApJSS*, 189, 270
 da Cunha, E., Charlot, S., & Elbaz, D. 2008, *MNRAS*, 388, 1595
 Daddi E., Dickinson, M., Morrison, G., et al. 2007, *ApJ*, 670, 156
 de Barros, S., Schaerer, D., Stark, D.P. 2012, arXiv:1207.3663
 Elbaz, D., Dickinson, M., Hwang, H.S., et al. 2011, *A&A*, 533, 119
 Fontanot, F., De Lucia, G., Monaco, P., Somerville, R. S., & Santini, P. 2009, *MNRAS*, 397, 1776
 Finkelstein, F.S., Papovich, C., Salmon, B., et al. 2011, *ApJ*, 756, 164
 Heinis, S., Buat, V., Bethermin, M., et al. 2013, in preparation
 Kennicutt, R.C. 1998, *ARA&A* 36, 189
 Kennicutt, R.C. & Evans, N.J. 2012, *ARA&A* 50, 531
 Kobayashi, M. A. R., Inoue, Y., & Inoue, A. K. 2013, *ApJ*, 763, 3
 Maraston, C., Pforr, J., Renzini, A., et al. 2010, *MNRAS*, 407, 830
 Marchesini, D., van Dokkum, P. G., Förster Schreiber, N. M., et al. 2009, *ApJ*, 701, 1765
 Noeske, K. G., Weiner, B. J., Faber, S. M., et al. 2007, *ApJ*, 660, L43
 Noll, S., Burgarella, D., Giovannoli, E., et al. 2009, *A&A*, 507, 1793
 Papovich, C., Dickinson, M., & Ferguson, H. C. 2001, *ApJ*, 559, 620
 Pforr, J., Maraston, C., & Tonini, C. 2012, *MNRAS*, 422, 3285
 Pilbratt, G., Riedinger, J.R., Passvogel, T., et al. 2010, *A&A* 518, L1
 Poglitsch, A., Waelkens, C., Geis, N., et al. 2010, *A&A*, 518, L2
 Reddy, N., Pettini, M., Steidel, C. et al. 2012, *ApJ*, 754, 25
 Rodighiero, G., Daddi, E., Baronchelli, I., et al. 2011, *ApJ*, 739, L40
 Sargent, M. T., Bethermin, M., Daddi, E., & Elbaz, D. 2012, *ApJ*, 747, L31
 Schaerer, D., de Barros, S., Sklias, P. 2013, *A&A* 549, 4